Journal of Membrane Science 586 (2019) 34–43

Contents lists available at ScienceDirect

Journal of Membrane Science

journal homepage: www.elsevier.com/locate/memsci

Defect-free high-silica CHA zeolite membranes with high selectivity for light gas separation

Pelin Karakiliç[a], Xuerui Wang[b], Freek Kapteijn[b], Arian Nijmeijer[a], Louis Winnubst[a,*]

[a] Inorganic Membranes, MESA + Institute for Nanotechnology, University of Twente, P.O. Box 217, 7500, AE Enschede, the Netherlands
[b] Catalysis Engineering, Chemical Engineering Department, Delft University of Technology, Van der Maasweg 9, 2629, HZ Delft, the Netherlands

ARTICLE INFO

Keywords:
Zeolite membrane
CHA zeolite
SSZ-13
Natural gas purification
SF_6 recovery

ABSTRACT

A systematic approach is described for the fabrication of defect-free high-silica zeolite membranes with CHA (SSZ-13) topology. Home-made hydrothermally-synthesized CHA seeds were coated on porous α-alumina substrates with a pore diameter of 80 nm and by means of a further hydrothermal treatment a zeolite membrane layer was formed. In order to obtain a thin and defect-free zeolite layer, the influence on the final microstructure of seed concentration during coating, coating method (rubbing, dip- or spin-coating) and crystal growth time was investigated. The template removal procedure was optimized to avoid the formation of cracks or defects. For an optimal thermal treatment, using a step-wise temperature increase to 500 °C, the membranes exhibit CO_2/CH_4 permselectivities of 25–30 with CO_2 permeances of around 2 x 10^{-7} mol m^{-2} s^{-1} Pa^{-1} at 22 °C and 2 bar of pressure difference. O_2 plasma pre-treatment prior to template removal increased the CO_2/CH_4 permselectivity to 176, while maintaining the same CO_2 permeance values when no pre-treatment was used. The SF_6 permeances, both at low (22 °C) and high (200 °C) temperatures, were below the detection limit (2 x 10^{-10} mol m^{-2} s^{-1} Pa^{-1}), which in return results in very high N_2/SF_6 permselectivities of more than 700.

1. Introduction

Zeolite membranes have great potential for the separation of liquids and gases thanks to their high thermal, chemical and mechanical stability as well as their uniform and molecular-sized pore structures, which is unique for each type of framework. Among the 235 different zeolite frameworks with a unique porous structure, only around 10 were studied as zeolite membrane material. The CHA-type framework has a 3-dimensional interconnected pore system with 8-membered rings and one of the smallest pore size (0.38 × 0.38 nm) for zeolite structures used as membrane material. Depending on the elemental structure, CHA has three analogues: low silica (chabazite), high-silica (SSZ-13) and silicoaluminophosphate-34 (SAPO-34) which are widely used for catalytic applications [1,2] and separations [3,4].

High-silica zeolites are the most thermal-stable ones (up to 800 °C), since more energy is necessary to break the Si-O bond than the Al-O bond [5]. In addition, high-silica zeolites are found to be less defective, and therefore more suitable for gas separation [6]. Furthermore, high-silica zeolites are more hydrophobic that would minimise the need of completely drying the feed gas and have better performance for the separation of CO_2/CH_4 gas mixtures [7].

High-silica (SSZ-13) CHA zeolites were prepared using various silica precursors such as colloidal silica LUDOX AS-40 [8], monomeric tetraethyl orthosilicate (TEOS) [9,10], and fumed silica Cab-O-Sil® M5 [11] by using N,N,N-trimethyl-1-adamantammonium ($TMAda^+$) as structure directing agent (SDA) at temperatures ranging from 135 to 170 °C.

High separation performances and maximization of the product flux can be accomplished by fabricating thin, defect-free and oriented zeolite layers in a reproducible manner, which is regarded as the main challenge for large-scale implementation of the zeolite membrane separation technology in the chemical industry. The defect formation during the fabrication of zeolite membranes is often inevitable [12]. Grain boundary (intercrystalline) defects form while growing the seed crystals into a zeolite layer, which correspond to micropore or mesopore defects [13]. In addition, during the template removal by temperature treatments, pinholes or cracks (macropore defects) form due to the mismatch in thermal expansion coefficient (CTE) between zeolite layer and substrate [14,15]. Formation of these defects, which have larger sizes than the pore openings of zeolite crystals, results in low selectivity in gas separation as gases simply permeate through these defects without being rejected by the separation layer. Besides, the CHA structure is more prone to have defects during thermal treatments as its accessible volume of 17.27% [16] for the template is much higher than

* Corresponding author.
E-mail address: a.j.a.winnubst@utwente.nl (L. Winnubst).

https://doi.org/10.1016/j.memsci.2019.05.047
Received 9 April 2019; Received in revised form 17 May 2019; Accepted 18 May 2019
Available online 22 May 2019

that of other zeolite frameworks such as MFI (9.81%) and DDR (9.21%). The higher template loading creates higher stress during detemplation, which causes difficulties in fabricating defect-free SSZ-13 CHA films [17].

The most commonly used method to overcome the formation of grain boundary defects in zeolite membranes is rapid thermal processing (RTP) instead of a conventional calcination [18–20]. Additionally, various post-treatment methods were widely studied to reduce the defects density, e.g. by filling defects with various chemicals, surfactants or sols [21–23]. Besides, ozonication is used as a detemplation technique where an oxygen/ozone mixture (approximately 2% ozone) is brought into contact with the zeolite layer at elevated temperatures (around 250 °C) at which ozone decomposes into atomic oxygen and radical species, which are highly reactive, remove the SDA by oxidation. In this way crack formation as a result of high calcination temperatures is avoided [17,24,25]. Finally, ultraviolet irradiation was also used to decompose and remove the SDA from the pores of SSZ-13 hollow fiber membranes [26]. This is a rather easy process as it can be done in ambient air as the ultraviolet irradiation excites the SDA and forms activated species that would react with oxygen to form molecules such as CO_2, H_2O and N_2.

In this paper we report a detailed study on fabrication of thin and defect-free high-silica (SSZ-13) CHA zeolite membranes by controlling many important parameters in the synthesis such as the seeding method, seed concentration, crystal growth time, and template removal conditions. The membranes exhibit high separation selectivities which are necessary for light gas separation applications such as CO_2/CH_4 separation in natural gas purification and also for SF_6 recovery. SF_6 is indispensably used as insulating gas in the electrical transmittance systems thanks to its high dielectric and arc-quenching properties [27], and has to be recovered from N_2 due to its high global warming potential (23,900 times greater than that of CO_2) which makes it an extremely potent greenhouse gas [27].

O_2 plasma was also applied as a pre-treatment technique before the thermal removal of the SDA. Although studied for detemplation of zeolite samples, this is the first paper discussing the effect of O_2 plasma as a pre-treatment method on the permeance and separation performance of SSZ-13 membranes. Thus, more understanding on developing defect-free SSZ-13 membranes is gained, resulting in a reproducible fabrication of SSZ-13 zeolite membranes, which brings these SSZ-13 membranes a step further to commercial gas separation application.

2. Experimental

2.1. Membrane fabrication

The macroporous, polished and disc-shaped α-alumina supports with 39 mm diameter, 2 mm thickness, 35% porosity and 80 nm pore diameter are obtained from Pervatech B.V. the Netherlands.

The SSZ-13 high-silica CHA seeds were synthesized using the recipe of Yarulina et al. [28] with some adaptations. A seed precursor solution was prepared by using fumed silica (CAB-O-SIL® M-5, Cabot) as silica precursor, N,N,N-trimethyl-1-adamantammonium hydroxide (TMAdaOH, 25% in water, SACHEM, Inc.) as Structure Direction Agent (SDA), sodium hydroxide pellets (NaOH, ≥ 97%, Sigma Aldrich), sodium aluminate ($NaAlO_2$, Sigma Aldrich) and deionized water. TMAdaOH, NaOH, $NaAlO_2$ and H_2O were mixed in a PTFE beaker and stirred with a magnetic stirrer (900 rpm) at room temperature until the total dissolution of NaOH and $NaAlO_2$. After addition of fumed silica the mixture was stirred for 6 h to form a gel with a molar composition of 1 SiO_2: 0.19 TMAdaOH: 0.18 NaOH: 0.02 $NaAlO_2$: 42.75H_2O. This gel mixture was poured in a 125 mL Teflon-lined stainless steel autoclave (Parr Instrument Company) and the hydrothermal synthesis took place at 160 °C for 6 days. The obtained seed crystals were recovered through wash, centrifuge and ultrasonic treatments. These treatments were repeated until the solution became pH neutral (pH of the supernatant between 7-8). The seeds were dried at 110 °C overnight in a BINDER FED 56 drying oven and calcined in an air furnace at 650 °C for 8 h with a heating and cooling rate of 1 °C/min for removing the SDA template. These initial hydrothermally-synthesized seeds were used for further seed fabrication, in order to shorten the synthesis time from 6 days to 3 days, as also reported by Yang et al. [26]. During this seed-assisted CHA seed synthesis, 2 mL of an aqueous solution of 0.125 wt% seeds was added to the 6 h-aged gel mixture, as described above, and this gel was aged for another 15 min, subsequently treated in an autoclave for 3 days at 160 °C and finally washed, dried and calcined as described above.

After synthesis and template removal from the seeds via calcination, the seeds were deposited on α-Al_2O_3 substrates via rubbing, spin-coating or dip-coating using a water suspension having different concentration of seeds (0.25, 0.125 and 0.0625 wt% seeds). Rubbing was done using Latex gloves and rubbing the seed crystals on the support surface. For spin coating a WS-400B-6NPP/LITE spin-coater (Laurell Technologies Corporation) was used at 2500 rpm for 30 s. Clean-room conditions (class 100) were used for dip-coating of the seeds and the porous supports were brought to contact with the seed containing solution using a dip-coater (Velterop DA 3960/02) with an angular dipping rate of 0.06 rad s^{-1}. After coating the substrates, the seed-coated discs were dried overnight at 110 °C and stored under ambient conditions until the seed growth.

The seed growth solution, used for membrane layer formation, was prepared by using a lower amount of $NaAlO_2$ than for the solution used for seed synthesis, to reduce the Si/Al ratio of the final zeolite layer. In this case the mixture had a molar composition of 1 SiO_2: 0.19 TMAdaOH: 0.18 NaOH: 0.01 $NaAlO_2$: 42.75H_2O and after aging for 6 h it was poured into the autoclave. The seed-coated substrates, of which the sides and bottom were wrapped with PTFE tape so that the zeolite crystals were only formed on the seed-coated layer, were placed in the autoclave vertically. The reaction temperature was kept at 160 °C and crystal growth times of 5, 9, 18, 36, 72 and 144 h were used. Then, the membranes were washed with an excess amount of water and dried at 110 °C overnight.

The membranes were calcined under air to remove the structure directing agent at two different heating programs, one at temperature of 500 °C for 2 h with intermediate dwells of 2 h at 400 and 450 °C and a second one at 600 °C with 8 h of dwell time without intermediate dwell. In both cases heating and cooling rates of 0.5 °C/min were used.

Additionally, O_2 plasma as a pre-treatment prior to calcination was applied to relax the layer for the removal of the structure directing agent from the pores of the membranes without causing defect-forming stress on the zeolite layer. An oxygen plasma is supplied by a Femto low-pressure plasma cleaner (Diener) with an oxygen pressure of 1.00 mbar applied during a plasma treatment of 15 min.

2.2. Characterization

The X-ray diffraction (XRD) patterns of the seed crystals and zeolite membranes were analysed by a Bruker D2 Phases X-ray diffraction with Cu-$K\alpha$ radiation (λ = 1.5418 nm) in the 2θ range of 5–90°, using steps of 0.02°. The normalized reflections were compared with the reported reference patterns from the International Zeolite Association [16].

The elemental composition (Si/Al ratio) of the SSZ-13 zeolite seeds were monitored by a Bruker S8 Tiger X-ray Fluorescence (XRF) using QUANT-EXPRESS analysis method.

The particle size distribution (PSD) of zeolite seed crystals that were synthesized and used in the coating suspension was analysed by a Malvern Zetasizer Nano ZS instrument using dynamic light scattering (DLS) technique.

Thermogravimetric analysis (TGA) in air was performed on a STA 449F3 Jupiter® (Netzch) to measure the weight loss of the uncalcined seeds as a function of temperature to determine the optimal thermal treatment for the removal of the SDA. A blank correction with an empty

TGA cup were carried out prior to the TGA analysis.

To envisage the coverage of the seeds after the seed-coating step, the samples were analysed by a KEYENCE VK-9700 3D laser scanning confocal microscope (LSCM).

The size and shape of the synthesized seeds as well as the thickness and the surface morphology of the grown zeolite layer were analysed by a JEOL JSM 6010LA scanning electron microscope (SEM) at an acceleration voltage of 5 kV. The SEM was equipped with an energy dispersive X-ray spectrometer (EDX) to have a semi-quantitative elemental analysis of the samples. Prior to the SEM analysis, the samples were sputter-coated with a 5 nm chromium layer.

The gas permeability of the membranes was analysed by a Convergence OSMO single gas permeation set-up working in a dead-end mode. Details of the set-up are given in Ref. [29]. During a measurement, the permeate side was kept at 1 bar and the gas feed pressure was varied to work at different transmembrane pressure (TMP = P_{feed} − $P_{permeate}$). The zeolite layer was placed facing the feed side. The pure gas permeances of He (hydrodynamic diameter 0.255 nm), H_2 (0.289 nm), CO_2 (0.33 nm), N_2 (0.364 nm), CH_4 (0.389 nm) and SF_6 (0.55 nm) were measured by mass flow meters.

X-ray photoelectron spectroscopy (XPS) was used to collect the element specific binding energies from the outermost 3–5 nm of a sample. The data was obtained with a Quentera SXM (scanning X-ray microscope) XPS from Physical Electronics using an Al-*Kα* source of 1486.6 eV.

3. Results and discussion

3.1. Seed crystal characteristics

XRD analysis (Fig. 1) confirms that the seed crystals have the high-silica CHA (SSZ-13) topology, based on the verified XRD pattern of SSZ-13 [30].

The elemental composition of the SSZ-13 crystals determined by XRF yielded a Si/Al ratio of 142 (99.3% Si and 0.7% Al). Both XRD and XRF results confirm that the seed crystals have the targeted high-silica (SSZ-13) CHA structure.

The particle size distribution of the seed crystals measured by DLS (Fig. 2) shows a monodispersed size of seed crystals in the range of 1 µm, indicating that the seeds are suitable for coating on alumina substrates which have a pore diameter of 80 nm.

In addition, the SSZ-13 seed crystals analysed by SEM (Fig. 3) were found to have the expected cubic shape with an average diameter of 1 µm, in agreement with DLS.

The supports were seeded by one of the attachment methods: dip-coating, spin-coating or rubbing. From the coverage of the seed crystals as observed via laser scanning confocal microscopy and shown in Fig. 4, dip-coating was found to be the better and more reproducible seed application technique.

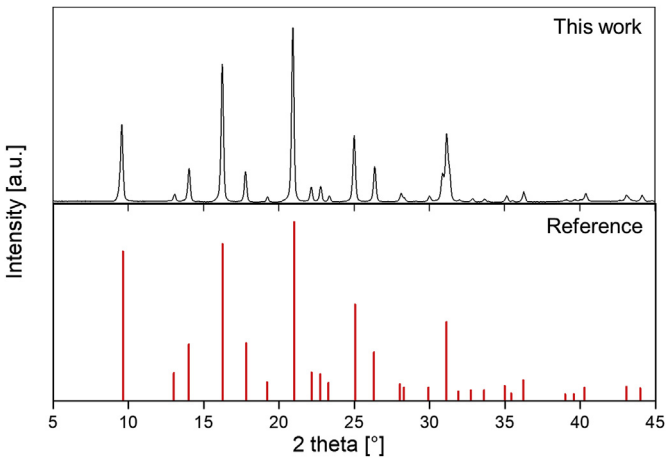

Fig. 1. *X-ray diffraction patterns of synthesized high-silica CHA (SSZ-13) seed crystals and comparison with literature* [30].

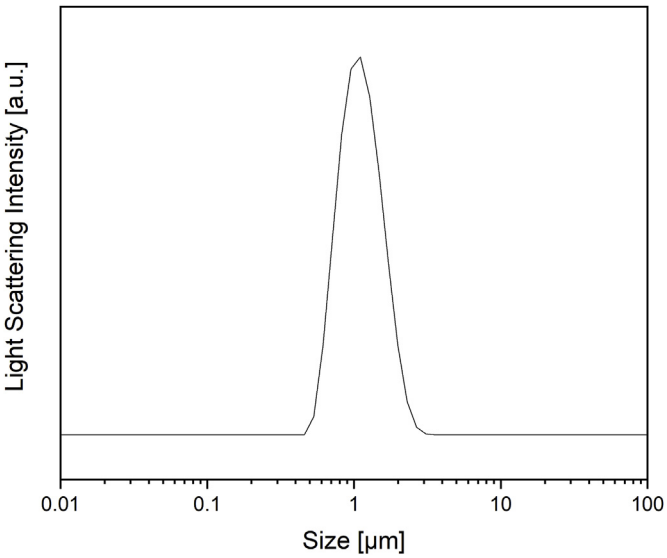

Fig. 2. Dynamic light scattering intensity of the SSZ-13 seed crystals.

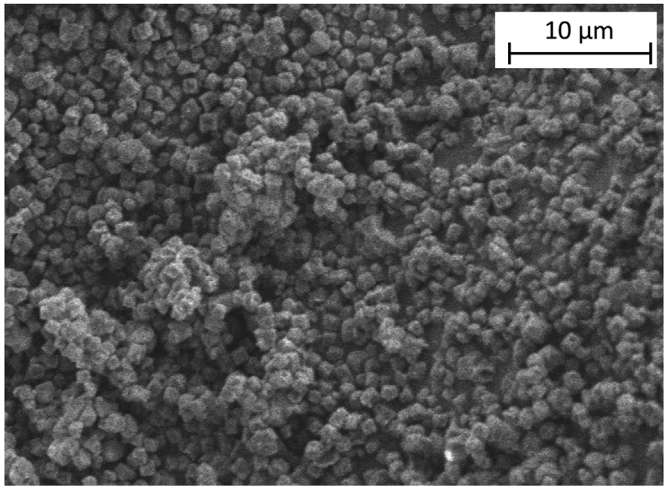

Fig. 3. SEM image of the synthesized SSZ-13 seed crystals.

Therefore, the membrane supports were further dip-coated with aqueous suspensions containing 0.25, 0.125 or 0.0625 wt% of seed crystals.

3.2. Membrane fabrication and its characteristics

After the attachment of the seed crystals by dip-coating with three different seed concentrations (0.25, 0.125 and 0.0625 wt%), the seeds were grown into a complete CHA layer for 144, 72, 36 or 18 h and for the low concentration also 9 and 5 h. In this way several experimental conditions were studied in order to get insight in the most optimal experimental conditions for making a complete, uniform, thin and defect-free zeolite layer. These samples will be referred by using the sample codes as given in Table 1.

After hydrothermally growing the attached seed crystals, the zeolite membranes were subjected to a gas permeation measurement to determine their gas tightness. If the membranes are impermeable, the defect-free nature of the zeolite layer prior to the thermal treatment is shown and the membranes can be brought to the next step: temperature treatment for SDA removal.

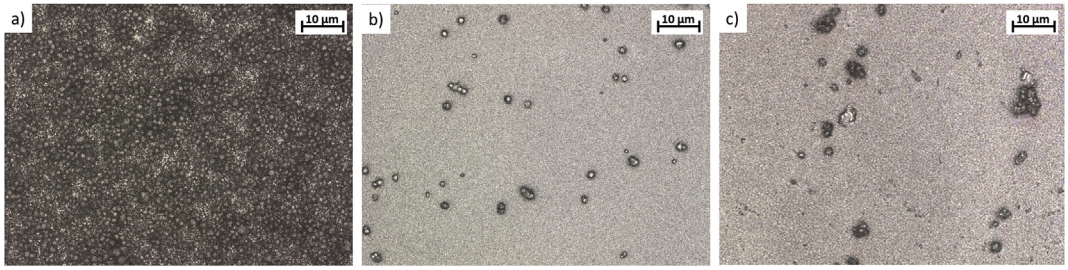

Fig. 4. Confocal microscopy images of the SSZ-13 on the alumina substrate to indicate the seed crystal coverage as applied via a) dip-coating, b) spin-coating and c) rubbing using 0.25 wt% seed concentration.

Table 1
Sample designations based on their seed concentrations and growth time.

Seed Concentration [wt.%]	Secondary growth time [h]	Sample code
H: high, 0.25 wt%	144	S-H-144
H: high, 0.25 wt%	72	S-H-72
H: high, 0.25 wt%	36	S-H-36
H: high, 0.25 wt%	18	S-H-18
M: medium, 0.125 wt%	144	S-M-144
M: medium, 0.125 wt%	72	S-M-72
M: medium, 0.125 wt%	36	S-M-36
M: medium, 0.125 wt%	18	S-M-18
L: low, 0.0625 wt%	144	S-L-144
L: low, 0.0625 wt%	72	S-L-72
L: low, 0.0625 wt%	36	S-L-36
L: low, 0.0625 wt%	18	S-L-18
L: low, 0.0625 wt%	9	S-L-9
L: low, 0.0625 wt%	5	S-L-5

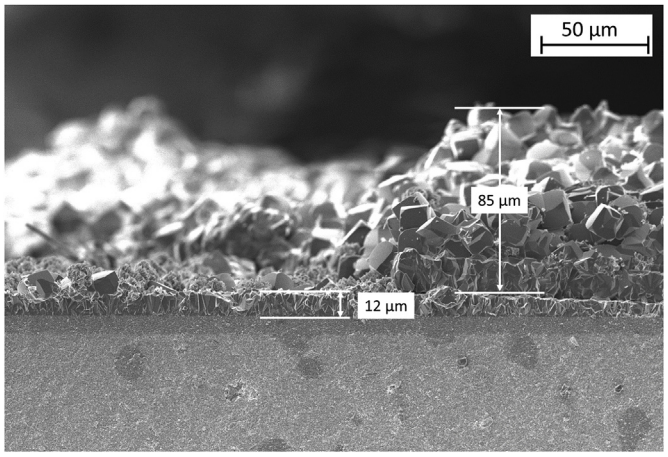

Fig. 5. Cross-sectional SEM image of S-H-144 showing the primary layer with thickness of 12 µm and a secondary layer with thickness of 85 µm.

An SEM image of the S-H-144 is shown in Fig. 5. The main layer has a thickness of 12 µm which was formed by the growth of the seed crystals for 144 h. Clearly a secondary layer is formed, having a thickness of 85 µm. This secondary layer is due to the formation of crystals in the seed growth solution. Further deposition of secondary crystals on the already seeded support is also observed in the literature [31]. All membranes with high seed coating concentration (H) broke in the membrane module of the gas permeation set-up upon exposure to gases even without applying any thermal treatment because of the thick layer (almost 100 µm; see Fig. 5). Even the minor forces applied on these membranes, caused by sealing it in the permeation set-up and applying a gas pressure of 2 bar, are sufficient to completely fracture the membrane. Therefore, the S-H membranes were found to be vulnerable to any mechanical stress and were not used for further investigations. So, further results and discussions only concern the S-M and S-L samples.

First of all the elemental composition of the membranes were analysed by EDS point analysis to determine the Si/Al ratio of the grown zeolite layers. It is found that the Si/Al ratio is varying between 50 and 60 proving the desired high-silica content of the SSZ-13 membrane layers [4,8,11].

The crystal structure of zeolite layers, grown on medium- and low-seeded membrane supports, was analysed. All membranes gave the same XRD pattern, only showing the peaks belonging to SSZ-13 and the α-alumina support. An example is given in Fig. 6.

The membrane layers, formed by secondary growth from dip-coated layers with medium (0.125 wt%) and low (0.0625 wt%) seed concentrations, were found to be defect-free before thermal treatment. The gas permeance results of S-M-72 are given as an example in Fig. 7, showing no detectable permeation of the light gases, before removing the template (SDA) by thermal treatments, so indicating a defect-free layer. However, after a thermal treatment at 600 °C in air (with a dwell time of 8 h, and heating and cooling rate of 0.5 °C/min), the membranes did not exhibit any selectivity regarding the size of the gas molecules tested. The single-gas permeance values as given in Fig. 7 are more resembling the α-alumina indicating that the zeolite layer on top of the α-alumina support does not provide any gas selectivity and only yields some permeation resistance.

Therefore, the focus was put on determining the optimal conditions for the removal of the template from the membranes prepared with the medium and low concentration seeds in order to preserve their defect-free nature through the template removal step.

In literature, various template removal conditions, as discussed in

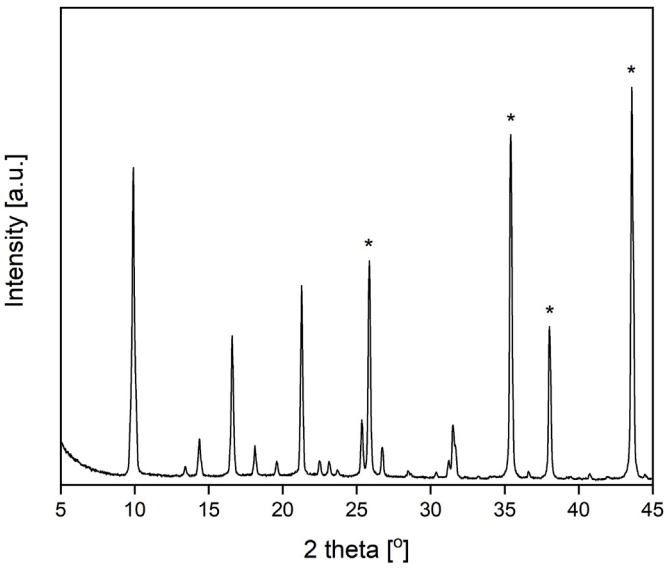

Fig. 6. XRD patterns of the grown SSZ-13 crystals on an alumina support with medium seeding (S-M-36). membranes Asterisk (*) represents the peaks origining from the α-alumina support.

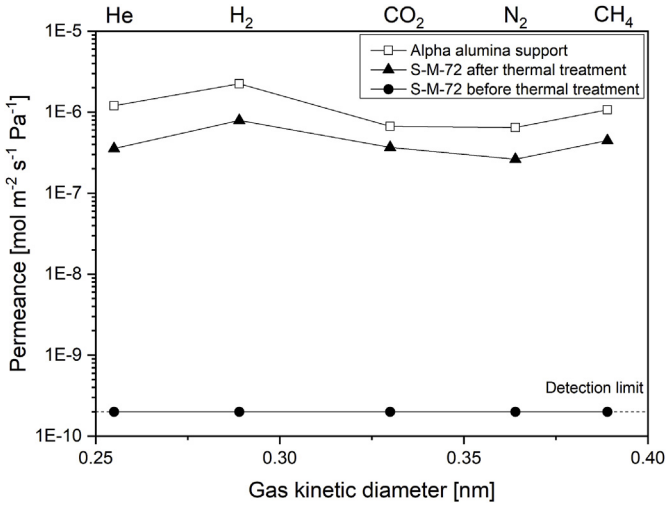

Fig. 7. Single gas permeances through S-M-72 membrane before and after thermal treatment at 600 °C (8 h; heating/cooling: 0.5 °C/min) and bare α-alumina support, measured at 22 °C and 2 bar of transmembrane pressure (lines are a guide to the eye).

Table 2
Template removal conditions from the SSZ-13 membrane pores.

Reference	Temperature [°C]	Dwell Time [h]	Heating Rate [°C/min]	Cooling Rate [°C/min]
[3]	580	12	0.5	0.5
[4]	480	6	0.5	0.5
[7] [a]	450	80	0.2	0.2
[10]	480	6	0.5	0.5
[28]	600	6	Not given	Not given
[32]	480	6	0.5	0.5
[33]	480	15	0.6	1.8

[a] Pure O_2 furnace. Rest: air furnace.

the introduction part of this paper, have been applied in addition to many different thermal treatment conditions. Details of thermal treatments, applied to SSZ-13 membranes, which resulted in defect-free membranes after thermal treatment, as confirmed by gas permeation tests, are given in Table 2.

Since different template removal temperatures in the range of 480–600 °C were used in the literature, it is important to find the optimal conditions for our synthesized material. Therefore, thermogravimetric (TGA) analysis was applied to investigate the weight loss of the as-synthesized zeolite seed crystals as a function of temperature and time. Fig. 8 shows the TGA results, using two different temperature programs: one with intermediate dwells for 1 h at every 50 °C (Fig. 8a) and one without intermediate dwell, and directly heated to 900 °C (Fig. 8b), using heat rate of 5 °C/min in both.

The weight loss due to the removal of water (up to 150 °C) is about 2%. Then, a slow weight loss occurs due to the partly decomposition of the SDA, $TMAda^+$, and it starts to completely decompose at around 400 °C in both cases, with and without intermediate dwell time. A weight loss of 18% (so up to a total sample weight loss of 20%) is an indication for the complete removal of the $TMAda^+$ as the accessible volume of CHA framework is given as 17.27% [16]. This weight loss is reached at lower temperatures (500 °C) in the system with intermediate dwell time (Fig. 8a) as it gives more time to oxidize the SDA whereas higher temperatures (600 °C) are required without intermediate dwells (Fig. 8b). Therefore, to avoid higher calcination temperatures which would result in defect formation and non-selective gas permeance (as shown in Fig. 7) due to the difference in the thermal expansion coefficients of the alumina substrate and the zeolite layer [17], the most suitable calcination conditions were analysed and it was shown that lower temperature would be sufficient to burn out the SDA by adding intermediate dwells.

So, the defect-free membranes were calcined at 500 °C for 2 h dwell time with additional intermediate dwells of 2 h at 400 and 450 °C, with a heating and cooling rate of 0.5 °C/min. These membranes preserved their defect-free nature by having no SF_6 (which has a larger kinetic diameter, 0.55 nm, than the pore size of SSZ-13, 0.38 nm) permeance as measured at 2 bar and 22 °C. The membranes exhibited size selective properties. The permeance values of He, H_2, CO_2, N_2 and CH_4, and CO_2/CH_4 permselectivities are given in Table 3.

The ideal CO_2/CH_4 permselectivities were quite similar for the membranes having different seed concentration during substrate coating and different secondary growth times (Table 3). The CO_2/CH_4 permselectivity (ideal selectivity) values are between 23 to 31, which are in the range (10–40) of the CO_2/CH_4 permselectivity values, reported in the literature for SSZ-13 membranes [33,34]. However, the differences in single-gas permeances were notable for the different membranes. This was expected considering the thickness of the membranes as a result of growth time. Both S-M and S-L membranes show higher permeances for all gases when the membranes were grown for 18 h as compared to those with 36 h of crystal growth. To confirm this idea and get more insight about the structure of these membranes, the cross-sections of the membranes were visually analysed by SEM (Fig. 9).

All SSZ-13 membrane layers were found to be compact and continuous on the α-alumina support.

The thickness was dominated by the crystal growth time instead of the seed concentration. Also, the thinner the zeolite layer, the more permeable the membrane.

The effect of a shorter crystal growth time of 9 (S-L-9) and 5 h (S-L-5) was investigated. In total, 6 membranes with synthesis method S-L-9 were prepared, and were all gas-tight prior to calcination by using the

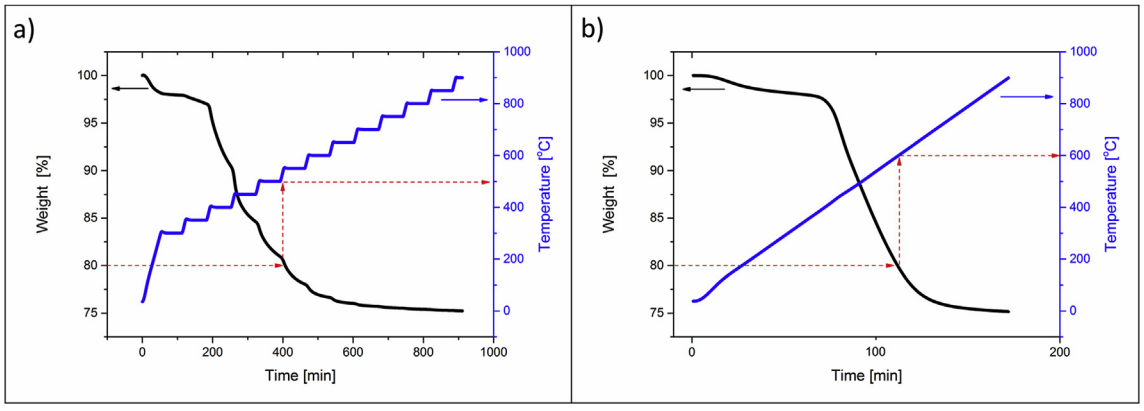

Fig. 8. Thermogravimetric analysis on SSZ-13 seed crystals using a heating rate of 5 °C/min a) with and b) without intermediate dwell time.

Table 3
Single gas permeances and CO_2/CH_4 permselectivities of the membranes (calcined at 500 °C with intermediate dwells) at 22 °C and 2 bar of transmembrane pressure.

Membranes	Gas Permeance [10^{-9} mol m^{-2} s^{-1} Pa^{-1}]					Permselectivity CO_2/CH_4
	He	H_2	CO_2	N_2	CH_4	
S-M-36	4.1	10	138	4.1	5.9	23
S-M-18	23	88	356	22	12	31
S-L-36	5.5	16	111	2.4	4.3	26
S-L-18	55	250	336	59	11	31
S-L-9	182	575	353	143	81	4

optimized temperature treatment. Their single gas permeance performance is provided in Table 3. SEM analysis of an S-L-9 sample indicated that in this case the SSZ-13 layer has a thickness of 1.8 μm (see Fig. 10).

The higher gas permeances through S-L-9 membranes (Table 3) could be a result of the thinner layer, 1.8 μm, due to shorter crystal growth time, or a more open structure by internal imperfections. Indeed, the CO_2/CH_4 permselectivity is not as high as the ones where the CH_4 permeance is lower due to the formation of a denser structure after a longer crystal growth time.

None of the four S-L membranes prepared with 5 h crystal growth time (S-L-5) were gas tight prior to the thermal treatment. Clearly, 5 h of secondary growth is insufficient for completely growing the seed crystals into a continuous layer. The gas permeances had a trend similar to the α-alumina support (see Fig. 7.) The SEM image of the surface of an as-synthesized S-L-5 membrane also shows the incomplete intergrowth to a continuous zeolite layer on the α-alumina support (Fig. 11).

These results give us the boundaries of fabrication of defect-free SSZ-13 zeolite layers. A too high seed concentration (S-H samples) or too short reaction time at low seed concentration (S-L-5) results in both cases in defective layers after synthesis. For the S-H samples this is caused by stresses because of a too thick zeolite layer, while for S-H-5 an incomplete CHA layer was formed. All other samples, as indicated in Table 1, gave a defect-free layer when a calcination treatment was given for 2 h at 500 °C, with intermediate dwells for 2 h at 400 and 450 °C. A lower seed concentration, but especially a reduction in crystal growth time, results in thinner zeolite layers with higher single gas permeances for the small gases. In conclusion, this study on material preparation provided us insight in the optimal fabrication of defect-free CHA membranes in a relatively fast way.

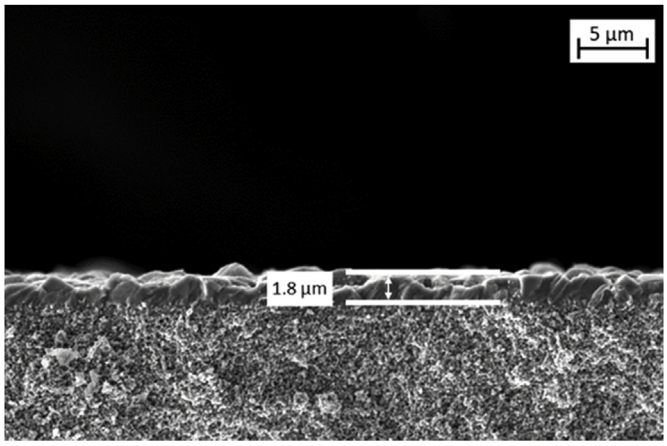

Fig. 10. Cross-sectional SEM image of S-L-9 membrane showing a zeolite layer thickness of 1.8 μm.

In addition to the room temperature tests, the gas permeances at elevated temperature (200 °C), while keeping a pressure difference of 2 bar, were measured. The single gas permeances through S-L-18 membranes at 22 °C (as tabulated in Table 3) and at 200 °C are compared in Fig. 12.

At 200 °C, higher permeance values for He, H_2, N_2 and CH_4 were obtained than at 22 °C due to the fact that the gas transport of these weakly adsorbing molecules increases at elevated temperatures, due to

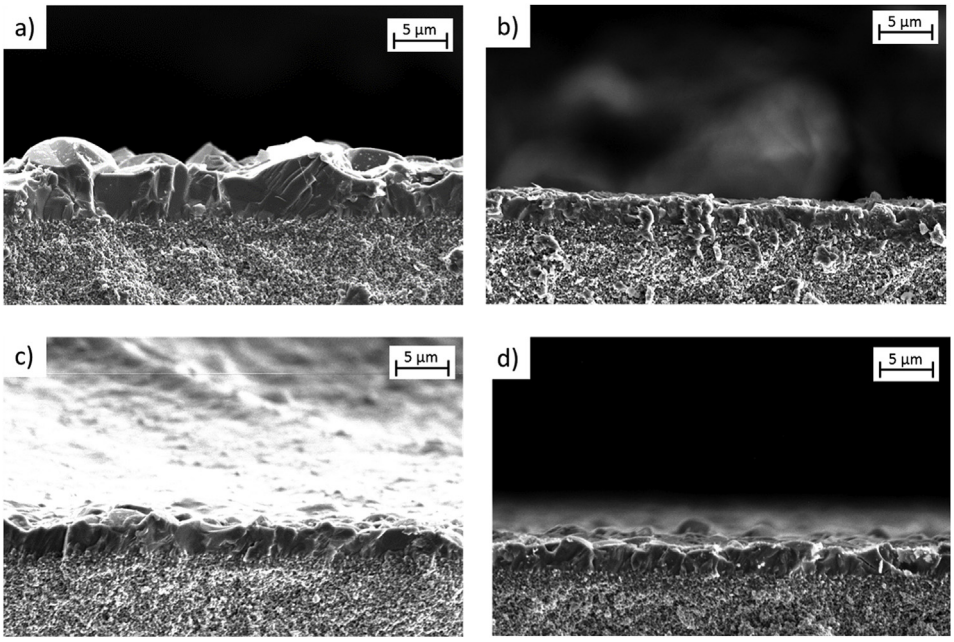

Fig. 9. Cross-sectional SEM images of a) S-M-36, b) S-M-18, c) S-L-36 and d) S-L-18. The thickness of the SSZ-13 layers is indicated (in μm).

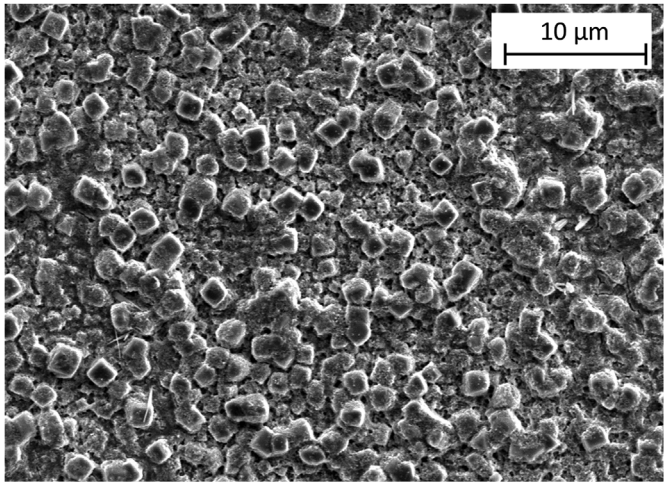

Fig. 11. SEM image of S-L-5 membrane showing the incomplete crystal growth into a continuous layer.

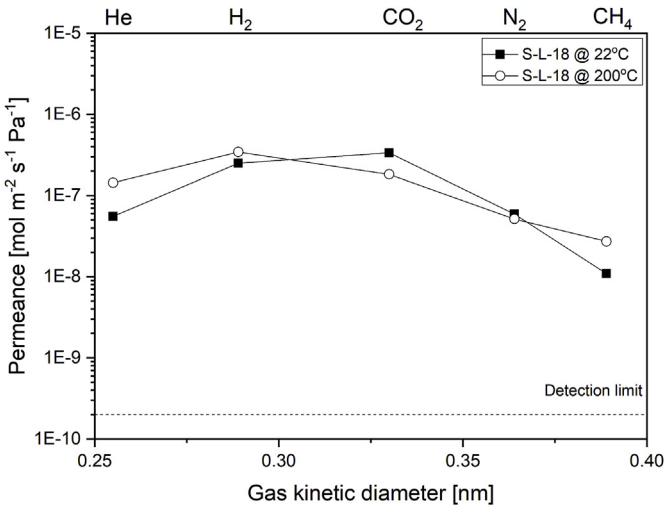

Fig. 12. The single gas permeances through S-L-18 membrane at 200 °C (open symbols) and 22 °C (solid symbols) with 2 bar of transmembrane pressure (lines are a guide to the eye).

an activated diffusion mechanism [35]. However, for CO_2, the permeance was slightly lowered because two phenomena contribute to its flux and have an opposite effect as a function of temperature. Adsorption and activated diffusion through the pores determine the CO_2 transport through CHA structures. As CO_2 is highly adsorbed on many zeolites including CHA [7,10], the high loading results in faster transport of CO_2 compared to the other components. At high temperatures this loading in the CHA decreases due to the exothermicity of adsorption, but the diffusivity increases. Since the increase of the latter is less than the decrease in loading the overall CO_2 permeance decreases with temperature. In the Henry regime the permeance activation energy is the sum of the adsorption enthalpy and the diffusivity activation energy.

$$E_{perm}^{app} = E_{diff} + \Delta H_{ads}$$

In case of the more bulky methane the diffusivity activation energy is larger than its heat of adsorption and overall the permeance increases with temperature. Similar observations have been made for DDR and MFI membranes [36,37].

So, at low temperatures, in SSZ-13 zeolites, a stronger adsorption of CO_2 than CH_4 is expected [38]. This adsorption behaviour, next to the molecular size effect, contributes to a higher CO_2 permeance than CH_4 resulting in a high permselectivity. However, at higher temperatures the opposite effects for CO_2 and CH_4 result in lower CO_2/CH_4 permselectivity values (6) than at 22 °C (31).

Table 4
Permselectivity values of light gases over SF_6 in S-L-18 membranes at 2 bar of pressure difference.

Gas Pair	Permselectivity[a]	
	22 °C	200 °C
H_2/SF_6	> 1250	> 1720
He/SF_6	> 280	> 720
CO_2/SF_6	> 1680	> 900
N_2/SF_6	> 300	> 260

[a] The SF_6 permeance was taken as the detection limit of the set-up (0.2 x 10^{-9} mol m^{-2} s^{-1} Pa^{-1}) for the permselectivity calculation.

Finally, the membrane selectivity of SF_6 with regard to the smaller gases was studied. All membranes were found to be SF_6 impermeable, both at low (22 °C) and high (200 °C) temperatures, meaning that SF_6 is completely rejected by the membranes. So, the light gas ideal permselectivities with regard to SF_6 were found to be very high for as shown in Table 4 (taking into account a detection limit of our gas permeation equipment of 0.2 x 10^{-9} mol m^{-2} s^{-1} Pa^{-1}).

These light gas permselectivities over SF_6 were found to be extremely high, especially for the N_2/SF_6 separation which is desired for SF_6 recovery.

The S-L-9 membranes were found to be SF_6 impermeable as well. The permeances of the light gases of S-L-9 (He, H_2, CO_2, N_2 and CH_4) show the highest values of all membranes investigated (see Table 3). A N_2 permeance of 143 x 10^{-9} mol m^{-2} s^{-1} Pa^{-1} was measured, while the detection limit of the set-up is 0.2 x 10^{-9} mol m^{-2} s^{-1} Pa^{-1}, meaning that for S-L-9 the N_2/SF_6 permselectivity was found to be more than 700. To the best of our knowledge this value is higher than ever reported in the literature [39–41].

The effect of eventual defects in the membrane is more obvious when higher pressures are used during permeation tests. Therefore, single gas permeance measurements at higher transmembrane pressures of 3, 4 and 5 bar were conducted on S-L-18 membranes, while keeping the temperature at 22 °C. The membranes were found SF_6 impermeable also at higher pressures. Moreover, almost identical CO_2/CH_4 permselectivities were observed at all transmembrane pressures. Thus, no significant effect of pressure on CO_2/CH_4 permselectivity was observed and the membranes remain impermeable for SF_6, which is another indication that defects are not present or present in very small amounts and small sizes.

3.3. Effect of O_2 plasma pre-treatment before calcination

Since the S-L-18 membrane had the highest CO_2/CH_4 permselectivity, this membrane was chosen to study the effect of an O_2 plasma treatment prior to the optimized temperature treatment at 500 °C with intermediate dwells for 2 h at 400 and 450 °C.

Also after the plasma pre-treatment the membranes were still impermeable to all of the gases. After the optimized thermal treatment for complete removal of the template the single gas permeances at 22 °C and 2 bar of pressure difference were determined (see Table 5).

For comparison, the single gas permeance values of S-L-18 samples with and without O_2 plasma pre-treatment are shown in Fig. 13.

The effect of O_2 plasma pre-treatment on gas permeances is remarkable. The 7–8 times lowered gas permeance values indicate that the pore structure is narrowed, and only the CO_2 permeance keeps similar values as compared to that of the direct thermal treated membranes. The strong decrease in methane permeance leads to a much higher CO_2/CH_4 permselectivity of 176 for the plasma treated membrane.

Table 5
The single gas permeances at 22 °C through S-L-18 membranes with O_2 plasma as a pre-treatment prior to optimized temperature treatment (low temperature, intermediate dwells).

Membranes	Gas Permeance [10^{-9} mol m^{-2} s^{-1} Pa^{-1}]					Permselectivity CO_2/CH_4
	He	H_2	CO_2	N_2	CH_4	
Without O_2 plasma	55	250	336	59	11	31
With O_2 plasma	8.1	37	260	8.1	1.5	176

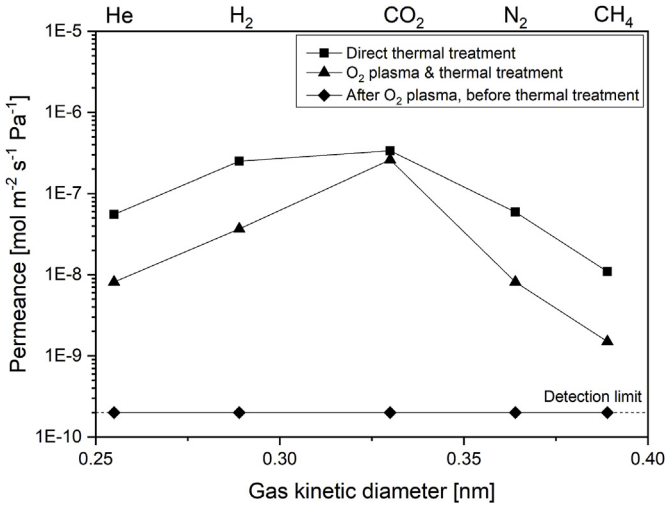

Fig. 13. Single gas permeance through S-L-18 membranes at 22 °C and 2 bar of pressure difference, after the membranes were exposed to either a direct thermal treatment (at 500 °C with intermediate dwells) or O_2 plasma and then a thermal treatment. Between O_2 plasma and thermal treatment, the membrane was impermeable. (Lines are a guide to the eye).

The following mechanism is proposed to occur during O_2-plasma and subsequent temperature treatment. During O_2 plasma pre-treatment, the methyl groups of the SDA, bonded to nitrogen (N) of the SDA (as seen in Fig. 14), are removed by the oxygen plasma [42,43] and as a result, the nitrogen atom becomes reactive. Besides, the oxygen plasma creates active Si-O- groups at the pore openings of the CHA structure. Subsequently, this is followed by a reaction of Si-O- with N to form a stable Si-O-N structure. During the temperature treatment after O_2 plasma, the large adamantyl group is burnt, which opens the pore. However, the Si-O-N bond is stable and remains after thermal treatment and causes a slight pore narrowing at the pore openings as schematically shown in Fig. 15.

Therefore, the gas permeances decrease while keeping the CO_2 permeance of the same order of magnitude as for non (O_2-plasma) pre-treated SSZ-13 membranes (Fig. 13) due to the high CO_2 adsorption capacity of SSZ-13 membranes [44] which governs its low temperature permeance. Hence, the narrowed pore opening as a result of O_2 plasma resulted in lower CH_4 permeance and consequently much higher CO_2/CH_4 permselectivities.

In order to verify this proposed mechanism, two SSZ-13 membranes, one with and one without O_2 plasma pre-treatment followed by calcination, were analysed by XPS in order to study the bonds in the N *1s* spectra (see Fig. 16).

The well-defined signal at 400 eV corresponds to nitrogen in C-N bonds [45] which is 85% of the nitrogen peak in the sample without O_2 plasma treatment and the small peak at 403.3 eV is tertiary amine [46]. However, the O_2 plasma treated membrane showed a secondary peak at 402.3 eV which is 64% of the total nitrogen peak area. This peak at 402.3 eV corresponds to N-O bonds [47] proving the prominent presence of N-O bonds in the zeolite layer after O_2 plasma treatment as suggested in Fig. 15.

In addition, crystal imperfections such as internal silanol defects [48], which are formed due to fast crystal growth [28], are presumably repaired by O_2 plasma, which would also yield a decrease in CH_4 permeance and therefore an increase in CO_2/CH_4 permselectivity.

4. Conclusions

High-silica (SSZ-13) CHA zeolite membranes were fabricated via a seeded growth method. Synthesis parameters, such as seed attachment method, seed concentration and seed crystal growth time, were optimized for the formation of thin and defect-free zeolite membranes. The thermal treatment for the removal of template was studied in detail. It was found that a temperature treatment at 500 °C for 2 h with intermediate dwells at 400 and 450 °C was the most optimal condition for synthesis of a defect-free CHA layer. These membranes exhibit good

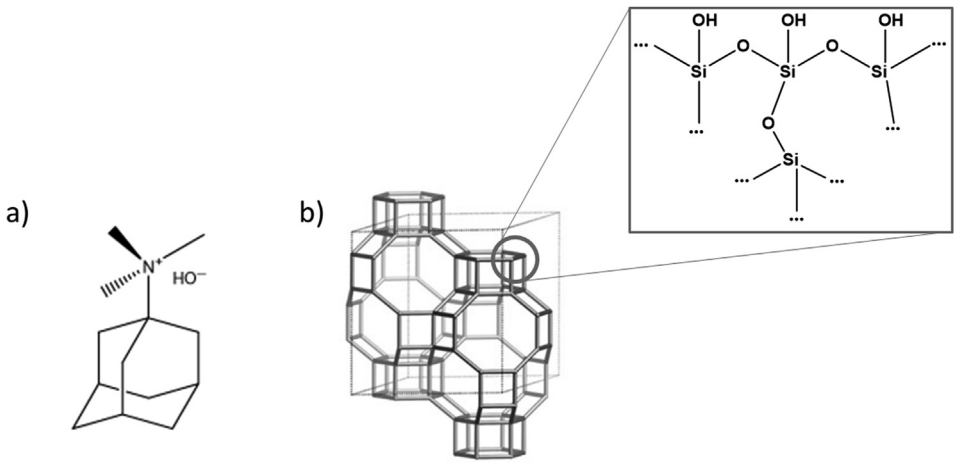

Fig. 14. a) the SDA (trimethyl adamantylammonium hydroxide) molecule and b) the CHA structure with enlarged the chemical structure, showing the silicon atoms connected to three oxygen atoms and one hydroxyl groups.

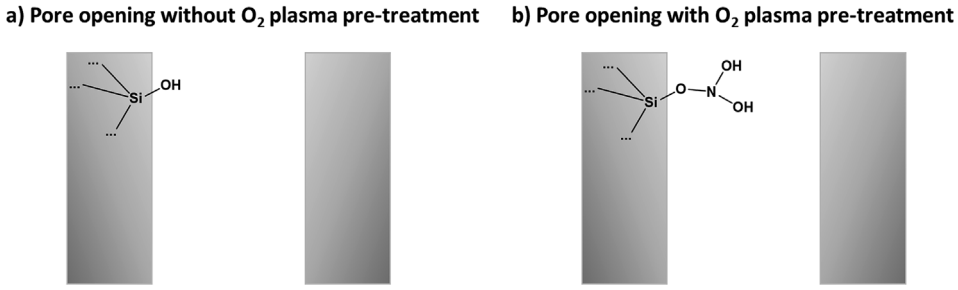

Fig. 15. Schematic presentation of the pore openings a) without and b) with O_2 plasma pre-treatment.

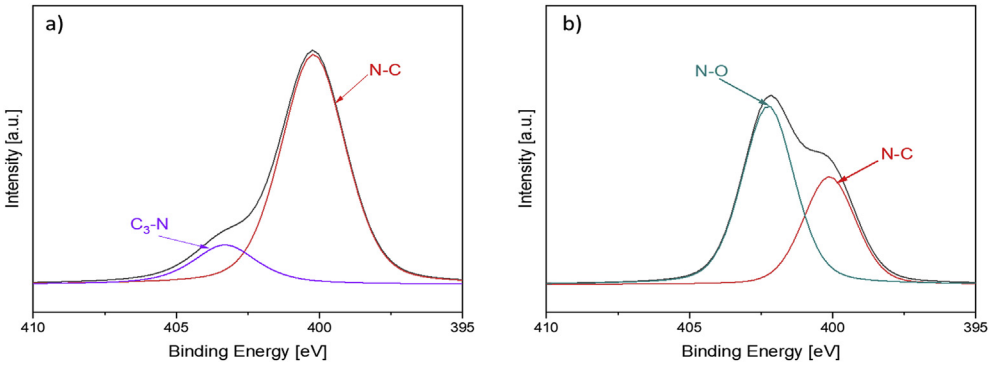

Fig. 16. XPS N 1s spectra of CHA membranes a) without b) with an O_2 plasma pre-treatment step, prior to the SDA removal.

size selective separation values. The best results in terms of CO_2/CH_4 separation performance were obtained with 0.065 wt% seeded membranes which were grown for 18 h. The membrane layer obtained with this procedure has a thickness of around 2 μm and exhibited a CO_2/CH_4 permselectivity of 30 at 22 °C and 2 bar of TMP with a CO_2 permeance of around 3.4 x 10^{-7} mol m^{-2} s^{-1} Pa^{-1}. In addition, 9 h grown 0.065 wt% seeded membranes were found to be more suitable for SF_6 recovery as these membranes were more permeable to the light gases whereas still impermeable to SF_6. Therefore, the permselectivities of light gases over SF_6 were found to be extremely high (N_2/SF_6 > 700) making these membranes suitable for SF_6 recovery both at room temperature and temperatures of at least 200 °C.

When the membranes were pre-treated with O_2 plasma prior to the temperature treatment, the pore openings are narrowed and the internal silanol imperfections are repaired. This denser and more ideal structure gives much higher CO_2/CH_4 permselectivity values reaching to 176, with similar CO_2 permeances of 1–3 x 10^{-7} mol m^{-2} s^{-1} Pa^{-1} but with much lower permeances of the other gases, compared to the non-plasma treated membranes. It is proposed that the O_2 plasma, combined with a temperature treatment, results in the formation of a Si-O-N bonding on the walls of the zeolite and subsequently in a pore narrowing if compared with non-O_2 plasma pre-treated membranes.

Conflict of interest

The authors declare no conflict of interest.

Acknowledgment

This research is supported by Netherlands Technology Foundation (STW-13941). The authors acknowledge Cindy Huiskes and Mieke Luiten-Olieman from University of Twente for their helpful discussion in this work, the department of Mechanics of Solids, Surfaces and Systems (MS3) from University of Twente for providing LSCM, Tom Velthuizen from University of Twente for X-ray Fluorescence (XRF) measurements, Gerard Kip from University of Twente for X-ray photoelectron spectroscopy (XPS) measurements and Frank Morssinkhof from University of Twente for technical support. Also, we would like to thank Cabot Corporation (Riga, Latvia) for providing us CAB-O-SIL ® M-5 high purity fumed silica for research purposes.

References

[1] Q. Zhu, J.N. Kondo, R. Ohnuma, Y. Kubota, M. Yamaguchi, T. Tatsumi, The study of methanol-to-olefin over proton type aluminosilicate CHA zeolites, Microporous Mesoporous Mater. 112 (2008) 153–161, https://doi.org/10.1016/j.micromeso.2007.09.026.

[2] G. Liu, P. Tian, J. Li, D. Zhang, F. Zhou, Z. Liu, Synthesis, characterization and catalytic properties of SAPO-34 synthesized using daaiethylamine as a template, Microporous Mesoporous Mater. 111 (2008) 143–149, https://doi.org/10.1016/j.micromeso.2007.07.023.

[3] K. Kida, Y. Maeta, K. Yogo, Pure silica CHA-type zeolite membranes for dry and humidified CO_2/CH_4 mixtures separation, Separ. Purif. Technol. 197 (2018) 116–121, https://doi.org/10.1016/j.seppur.2017.12.060.

[4] Y. Zheng, N. Hu, H. Wang, N. Bu, F. Zhang, R. Zhou, Preparation of steam-stable high-silica CHA (SSZ-13) membranes for CO_2/CH_4 and C_2H_4/C_2H_6 separation, J. Membr. Sci. 475 (2015) 303–310, https://doi.org/10.1016/j.memsci.2014.10.048.

[5] G. Cruciani, Zeolites upon heating: factors governing their thermal stability and structural changes, J. Phys. Chem. Solids 67 (2006) 1973–1994, https://doi.org/10.1016/j.jpcs.2006.05.057.

[6] J. Caro, M. Noack, P. Kölsch, Zeolite membranes: from the laboratory scale to technical applications, Adsorption 11 (2005) 215–227, https://doi.org/10.1007/s10450-005-5394-9.

[7] N. Kosinov, C. Auffret, G.J. Borghuis, V.G.P. Sripathi, E.J.M. Hensen, Influence of the Si/Al ratio on the separation properties of SSZ-13 zeolite membranes, J. Membr. Sci. 484 (2015) 140–145, https://doi.org/10.1016/j.memsci.2015.02.044.

[8] S.I. Zones, Zeolite SSZ-13 and its method of preparation, 4544538 US Pat, 1985.

[9] M.J. Diaz-Cabanas, P.A. Barrett, M.A. Camblor, Synthesis and structure of pure SiO_2 chabazite: the SiO_2 polymorph with the lowest framework density, Chem. Commun. (1998) 1881–1882, https://doi.org/10.1039/A804800B.

[10] K. Kida, Y. Maeta, K. Yogo, Preparation and gas permeation properties on pure silica CHA-type zeolite membranes, J. Membr. Sci. 522 (2017) 363–370, https://doi.org/10.1016/j.memsci.2016.09.002.

[11] E.A. Eilertsen, M.H. Nilsen, R. Wendelbo, U. Olsbye, K.P. Lillerud, Synthesis of high silica CHA zeolites with controlled Si/Al ratio, in: A. Gedeon, P. Massiani, F. Babboneau (Eds.), Stud. Surf. Sci. Catal. Elsevier B.V., 2008, pp. 265–268, , https://doi.org/10.1016/S0167-2991(08)80193-0.

[12] G. Bonilla, M. Tsapatsis, D.G. Vlachos, G. Xomeritakis, Fluorescence confocal optical microscopy imaging of the grain boundary structure of zeolite MFI membranes made by secondary (seeded) growth, J. Membr. Sci. 182 (2001) 103–109, https://doi.org/10.1016/S0376-7388(00)00549-4.

[13] H. Maghsoudi, Defects of zeolite membranes: characterization, modification and post-treatment techniques, Separ. Purif. Rev. 45 (2016) 169–192, https://doi.org/

10.1080/15422119.2015.1103270.
[14] M. Lassinantti Gualtieri, C. Andersson, F. Jareman, J. Hedlund, A.F. Gualtieri, M. Leoni, C. Meneghini, Crack formation in α-alumina supported MFI zeolite membranes studied by in situ high temperature synchrotron powder diffraction, J. Membr. Sci. 290 (2007) 95–104, https://doi.org/10.1016/j.memsci.2006.12.018.
[15] J. Dong, Y.S. Lin, M.Z.C. Hu, R.A. Peascoe, E.A. Payzant, Template-removal-associated microstructural development of porous-ceramic-supported MFI zeolite membranes, Microporous Mesoporous Mater. 34 (2000) 241–253, https://doi.org/10.1016/S1387-1811(99)00175-4.
[16] Database of Zeolite Structures (n.d.), http://www.iza-structure.org/databases/ , Accessed date: 27 April 2018.
[17] N. Kosinov, C. Auffret, V.G.P. Sripathi, C. Gücüyener, J. Gascon, F. Kapteijn, E.J.M. Hensen, Influence of support morphology on the detemplation and permeation of ZSM-5 and SSZ-13 zeolite membranes, Microporous Mesoporous Mater. 197 (2014) 268–277, https://doi.org/10.1016/j.micromeso.2014.06.022.
[18] W.C. Yoo, J.A. Stoeger, P.S. Lee, M. Tsapatsis, A. Stein, High-performance randomly oriented zeolite membranes using brittle seeds and rapid thermal processing, Angew. Chem. Int. Ed. 49 (2010) 8699–8703, https://doi.org/10.1002/anie.201004029.
[19] J.A. Stoeger, J. Choi, M. Tsapatsis, Rapid thermal processing and separation performance of columnar MFI membranes on porous stainless steel tubes, Energy Environ. Sci. 4 (2011) 3479–3486, https://doi.org/10.1039/c1ee01700d.
[20] J. Choi, H.-K. Jeong, M.A. Snyder, J.A. Stoeger, R.I. Masel, M. Tsapatsis, Grain boundary defect elimination in a zeolite membrane by rapid thermal processing, Science 325 (2009) 590–593, https://doi.org/10.1002/chin.200941223.
[21] G. Xomeritakis, Z. Lai, M. Tsapatsis, Separation of xylene isomer vapors with oriented MFI membranes made by seeded growth, Ind. Eng. Chem. Res. 40 (2001) 544–552, https://doi.org/10.1021/ie000613k.
[22] Y. Yushan, M.E. Davis, G.R. Gavalas, Preparation of highly selective zeolite ZSM-5 membranes by a post-synthetic coking treatment, J. Membr. Sci. 123 (1997) 95–103, https://doi.org/10.1016/S0376-7388(96)00206-2.
[23] D. Korelskiy, P. Ye, M.S. Nabavi, J. Hedlund, Selective blocking of grain boundary defects in high-flux zeolite membranes by coking, J. Mater. Chem. A. 5 (2017) 7295–7299, https://doi.org/10.1039/C7TA01268C.
[24] J. Kuhn, J. Gascon, J. Gross, F. Kapteijn, Detemplation of DDR type zeolites by ozonication, Microporous Mesoporous Mater. 120 (2009) 12–18, https://doi.org/10.1016/j.micromeso.2008.09.018.
[25] S. Heng, P.P.S. Lau, K.L. Yeung, M. Djafer, J.C. Schrotter, Low-temperature ozone treatment for organic template removal from zeolite membrane, J. Membr. Sci. 243 (2004) 69–78, https://doi.org/10.1016/j.memsci.2004.05.025.
[26] S. Yang, Y.H. Kwon, D.Y. Koh, B. Min, Y. Liu, S. Nair, Highly selective SSZ-13 zeolite hollow fiber membranes by ultraviolet activation at near-ambient temperature, ChemNanoMat 5 (2019) 61–67, https://doi.org/10.1002/cnma.201800272.
[27] A.A. Lindley, A. McCulloch, Regulating to reduce emissions of fluorinated greenhouse gases, J. Fluorine Chem. 126 (2005) 1457–1462, https://doi.org/10.1016/j.jfluchem.2005.09.011.
[28] I. Yarulina, A. Dikhtiarenko, F. Kapteijn, J. Gascon, Consequences of secondary zeolite growth on catalytic performance in DMTO studied over DDR and CHA, Catal. Sci. Technol. 7 (2017) 300–309, https://doi.org/10.1039/C6CY02307J.
[29] P. Karakiliç, C. Huiskes, M.W.J. Luiten-Olieman, A. Nijmeijer, L. Winnubst, Sol-gel processed magnesium-doped silica membranes with improved H_2/CO_2 separation, J. Membr. Sci. 543 (2017) 195–201, https://doi.org/10.1016/j.memsci.2017.08.055.
[30] L.T. Yuen, S.I. Zones, CHA SSZ-13 Si(93), Al(7), in: H. Robson, K.P. Lilleruc (Eds.), Verif. Synth. Zeolitic Mater. second ed., Elsevier Science B.V., 2001, pp. 126–128.
[31] P. Karakiliç, R. Toyoda, F. Kapteijn, A. Nijmeijer, L. Winnubst, From amorphous to crystalline: transformation of silica membranes into silicalite-1 (MFI) zeolite layers, Microporous Mesoporous Mater. 276 (2019) 52–61, https://doi.org/10.1016/j.micromeso.2018.09.020.
[32] T. Wu, M.C. Diaz, Y. Zheng, R. Zhou, H.H. Funke, J.L. Falconer, R.D. Noble, Influence of propane on CO_2/CH_4 and N_2/CH_4 separations in CHA zeolite membranes, J. Membr. Sci. 473 (2015) 201–209, https://doi.org/10.1016/j.memsci.2014.09.021.
[33] H. Kalipcilar, T.C. Bowen, R.D. Noble, J.L. Falconer, Synthesis and separation performance of SSZ-13 zeolite membranes on tubular supports, Chem. Mater. 14 (2002) 3458–3464, https://doi.org/10.1021/cm020248i.
[34] N. Kosinov, C. Auffret, C. Gücüyener, B.M. Szyja, J. Gascon, F. Kapteijn, E.J.M. Hensen, High flux high-silica SSZ-13 membrane for CO_2 separation, J. Mater. Chem. A. 2 (2014) 13083–13092, https://doi.org/10.1039/C4TA02744B.
[35] H. Li, K. Haas-Santo, U. Schygulla, R. Dittmeyer, Inorganic microporous membranes for H_2 and CO_2 separation—review of experimental and modeling progress, Chem. Eng. Sci. 127 (2015) 401–417, https://doi.org/10.1016/j.ces.2015.01.022.
[36] F. Kapteijn, J.M. van de Graaf, J.A. Moulijn, One-component permeation maximum: diagnostic tool for silicalite-1 membranes? AIChE J. 46 (2000) 1096–1100, https://doi.org/10.1002/aic.690460521.
[37] J. van den Bergh, W. Zhu, J. Gascon, J.A. Moulijn, F. Kapteijn, Separation and permeation characteristics of a DD3R zeolite membrane, J. Membr. Sci. 316 (2008) 35–45, https://doi.org/10.1016/j.memsci.2007.12.051.
[38] Y. Luo, H.H. Funke, J.L. Falconer, R.D. Noble, Adsorption of CO_2, CH_4, C_3H_8, and H_2O in SSZ-13, SAPO-34, and T-type zeolites, Ind. Eng. Chem. Res. 55 (2016) 9749–9757, https://doi.org/10.1021/acs.iecr.6b02034.
[39] J.W. Choi, S. Lee, B. An, S.B. Kim, S.H. Lee, Separation of sulfur hexafluoride from a nitrogen/sulfur hexafluoride mixture using a polymer hollow fiber membrane, Water Air Soil Pollut. 225 (2014) 1807, https://doi.org/10.1007/s11270-013-1807-7.
[40] P.J. Kim, Y.W. You, H. Park, J.S. Chang, Y.S. Bae, C.H. Lee, J.K. Suh, Separation of SF_6 from SF_6/N_2 mixture using metal–organic framework MIL-100(Fe) granule, Chem. Eng. J. 262 (2015) 683–690, https://doi.org/10.1016/j.cej.2014.09.123.
[41] A. Nouri, M. Jafari, M. Kazemimoghadam, T. Mohammadi, Potential separation of SF6 from air using chabazite zeolite membranes, Chem. Eng. Technol. 37 (2014) 317–324, https://doi.org/10.1002/ceat.201300297.
[42] M.J. Owen, P.J. Smith, Plasma treatment of polydimethylsiloxane, J. Adhes. Sci. Technol. 8 (1994) 1063–1075, https://doi.org/10.1163/156856194X00942.
[43] S. Bhattacharya, A. Datta, J.M. Berg, S. Gangopadhyay, Studies on surface wettability of studies on surface wettability of poly (dimethyl) siloxane (PDMS) and glass under oxygen-plasma treatment and correlation with bond strength, J. Microelectromech. Syst. 14 (2005) 590–597, https://doi.org/10.1109/JMEMS.2005.844746.
[44] N. Kosinov, J. Gascon, F. Kapteijn, E.J.M. Hensen, Recent developments in zeolite membranes for gas separation, J. Membr. Sci. 499 (2016) 65–79, https://doi.org/10.1016/j.memsci.2015.10.049.
[45] S.R. Venna, M.A. Carreon, Amino-functionalized SAPO-34 membranes for CO2/CH4 and CO2/N2 separation, Langmuir 27 (2011) 2888–2894, https://doi.org/10.1021/la105037n.
[46] X. Sun, C. Brückner, Y. Lei, One-pot and ultrafast synthesis of nitrogen and phosphorus co-doped carbon dots possessing bright dual wavelength fluorescence emission, Nanoscale 7 (2015) 17278–17282, https://doi.org/10.1039/c5nr05549k.
[47] K. Yamamoto, Y. Koga, S. Fujiwara, XPS studies of amorphous SiCN thin films prepared by nitrogen ion-assisted pulsed-laser deposition of SiC target, Diam. Relat. Mater. 10 (2001) 1921–1926, https://doi.org/10.1016/S0925-9635(01)00422-8.
[48] E. Dib, J. Grand, S. Mintova, C. Fernandez, Structure-Directing Agent Governs the Location of Silanol Defects in Zeolites, (2015), pp. 7577–7579, https://doi.org/10.1021/acs.chemmater.5b03668.